Full-scale fire testing of battery electric vehicles

Kang, S., Kwon, M., Choi, J., & Choi, S. (2023). Full-scale fire testing of battery electric vehicles. *Applied Energy*, *332*, [120497]. https://doi.org/10.1016/j.apenergy.2022.120497

Link to publication record in Ulster University Research Portal

Published in:
Applied Energy

Publication Status:
Published online: 15/02/2023

DOI:
10.1016/j.apenergy.2022.120497

Document Version
Publisher's PDF, also known as Version of record

General rights
Copyright for the publications made accessible via Ulster University's Research Portal is retained by the author(s) and / or other copyright owners and it is a condition of accessing these publications that users recognise and abide by the legal requirements associated with these rights.

Take down policy
The Research Portal is Ulster University's institutional repository that provides access to Ulster's research outputs. Every effort has been made to ensure that content in the Research Portal does not infringe any person's rights, or applicable UK laws. If you discover content in the Research Portal that you believe breaches copyright or violates any law, please contact pure-support@ulster.ac.uk.

Download date: 07/01/2023

Applied Energy 332 (2023) 120497

Contents lists available at ScienceDirect

Applied Energy

journal homepage: www.elsevier.com/locate/apenergy

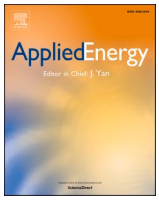

Full-scale fire testing of battery electric vehicles

Sungwook Kang [a], Minjae Kwon [a,b], Joung Yoon Choi [a], Sengkwan Choi [c,*]

[a] Fire Testing & Research Centre, Fire & Disaster Management Division, Korea Conformity Laboratories, Republic of Korea
[b] Advanced Functional Nanohybrid Material Laboratory, Department of Chemistry, Dongkuk University, Republic of Korea
[c] School of the Built Environment, Ulster University, UK

HIGHLIGHTS

- The characteristics of BEV fires is comparable with those of conventional passenger cars.
- The new combustibles in the battery pack make a minor contribution to the whole magnitude of BEV fires.
- The jet flame, caused by thermal runaway, accelerates the fire spread to other combustibles of BEVs.
- The uncertainties, induced from unforeseen thermal runaway and reignition, make a major risk to first responders.

ARTICLE INFO

Keywords:
Battery electric vehicle
Thermal runaway
Lithium-ion battery
Full-scale fire testing
Thermal behaviour

ABSTRACT

The market share of electric vehicles, powered by lithium-ion batteries (LIB), has been expanding worldwide with the global momentum towards green technology and improving the driving range on one full-charge. Studies are, however, still required on the fire safety of the latest but unmatured technology due to a distinctive phenomenon called thermal runaway. In this study, a series of full-scale fire experiments were conducted, focusing on the understanding of thermal behaviours of battery electric vehicle (BEV) fires. To provide up-to-date information on BEV fires, the latest BEV model with a high electric-energy capacity (64 kWh) was selected. For comparative analysis purposes, a LIB pack and a BEV body were tested individually after being physically disassembled. An internal combustion engine vehicle and a hydrogen fuel cell electric vehicle were also tested. During testing, the combustion of the BEV fires continued for approximately 70 min, resulting in critical measures of burning being determined; peak heat release rate (pHRR), total heat released (THR), fire growth parameter, and the average effective heat of combustion were measured to be 6.51–7.25 MW, 8.45–9.03 GJ, 0.0085–0.020, and 29.8–30.5 MJ/kg, respectively. It was also observed that the pHRR and THR were governed by the combustion characteristics of typical combustible materials in the passenger cabin, rather than by that of particular contents in the LIB pack with thermal runaway. Instead, a jet fire intensively discharging from the LIB pack led to a rapid flame spreading to adjacent combustible components of the BEV, thereby accelerating the fire growth. The findings could contribute to the activities of the first responders to BEV fire accidents, fire safety engineers, and structural member designers. This study also makes public the measured thermal quantities for further studies on the fire safety of existing or designing car-parking related structures.

1. Introduction

Greatest attention is currently focused on electric vehicles relying on electric battery energy as a power source, although the fundamental idea of these vehicles was invented in the 1800 s [1]. Their market share has been rapidly expanding against that of the conventional internal combustion engine vehicle (ICEV), as electric vehicles represent green technology as well as providing extraordinary driving performance. Electric vehicle sales, including those of plug-in hybrid electric vehicles (PHEV), globally reached 6.75 million units in 2021, approximately 10.1 % of the market share of car sales worldwide [2]. Concurrently, the capacity of electric vehicle battery packs has been gradually improving to meet the growing demand for a longer driving range on one full-charge; for example, in the U.S. market, the average capacity increased from 41.2 kWh in 2015 to 70.5 kWh in 2020 [3].

In 2006 a massive electronics industry recall occurred in the global laptop industries and in 2016 the production of an electronic device

* Corresponding author at: Belfast School of Architecture & the Built Environment, Ulster University, 2-24 York Street, Belfast BT15 1AF, UK.
E-mail address: s.choi@ulster.ac.uk (S. Choi).

https://doi.org/10.1016/j.apenergy.2022.120497
Received 8 October 2022; Received in revised form 20 November 2022; Accepted 3 December 2022
Available online 15 December 2022
0306-2619/© 2022 The Author(s). Published by Elsevier Ltd. This is an open access article under the CC BY license (http://creativecommons.org/licenses/by/4.0/).

Nomenclature

A	surface area [m^2]
c_p	specific heat [J/(kg.K)]
F	view factor
h	convection heat transfer coefficient [W/(m2.K)]
$\dot{m}$	mass loss rate [kg/s]
$\dot{Q}$	thermal energy [W]
$\dot{q}''$	heat flux [W/m^2]
T	temperature [K]
t	time [s]

Greek symbols

α	thermal absorptivity
ε	thermal emissivity
θ	growth parameter for t-square fires [MW/s^2]
ρ	density [kg/m^3]
Σ	Stefan-Boltzmann constant[$W/(m2.K^4)$]

Subscripts

end	end
f	fire
g	gauge
ini	initial
loss	loss
s	surface
∞	surroundings

Abbreviations

BEV	battery electric vehicle
FCC	fuel consumption calorimetry
FCEV	fuel cell electric vehicle
HRR	heat release rate
ICEV	internal combustion engine vehicle
LIB	lithium-ion battery
OCC	oxygen consumption calorimetry
PHEV	plug-in hybrid electric vehicle
pHRR	peak heat release rate
THR	total heat released

Table 1
Research objectives corresponding to specimen type from the fire safety viewpoint.

Level	Type of specimen	Research objectives
1	Component materials	Thermochemical/electrochemical characteristics of the unit
2	Single cell	Thermal characteristics of the unit under thermal/electrical/mechanical impact conditions, mechanism of gas venting and thermal runaway initiation, and quality/quantity of vent gas
3	Multiple cells /single module	Thermal characteristics of the unit under thermal/electrical/mechanical impact conditions, and cell-to-cell thermal runaway/heat propagation
4	Multiple modules	Module-to-module thermal runaway/heat propagation in horizontal and vertical directions
5	Pack	Thermal characteristics of the unit under thermal/electrical/mechanical impact conditions, and pack-to-vehicle body fire spread
6	Battery Electric Vehicle (BEV)	Magnitude of BEV fire hazards, and BEV-to-adjacent object fire spread

model was permanently ceased, due to thermal runaway incidents originating from the potentially faulty lithium-ion batteries (LIBs) [4–5]. Such occasions drew attention to research on LIB safety, as well as to relevant regulations and standards; several LIB safety related standards have been being developed and revised globally for cell-, module-, and even system-level LIBs, such as IEC, ISO, UN, SAE, UL, SAND and GB/T. As the technology on LIB system has not yet fully matured to date, unforeseen fire patterns have been widely reported at various international incidents associated with battery electric vehicles (BEVs). In South Korea, 17 local BEV-fire accidents occurred for the period between 2018 and 2021 [6]. In particular, 6 events happened in enclosed areas, such as manufacturing factories and underground car parks in buildings. Under such circumstances, more sever fire behaviour and subsequent damage were evaluated compared to those events that happened in open spaces. As a response to these new fire scenarios, comprehensive revision should be carried out on several technical aspects of design conditions, such as the fire degradation of loadbearing structures (of multi-storey car parks, underground spaces, and tunnels), the capacity of current fire suppression systems, and the applicability of the existing fire-suppression strategies, before BEVs become the majority of vehicles in societies.

In order to carry out these revisions, a list of key input parameters need to be preliminarily determined, in conditions of open and enclosed spaces respectively. The parameters are the rate of heat release (HRR in W) of a burning car, amount of total heat released (THR in J), fire growth coefficient (in W/s^2), fire load (in J/m^2), mass loss (i.e., fuel consumption), effective heat of combustion (in J/g), incident heat fluxes in the vicinity of the heat source (in W/m^2), flame spread throughout the burning vehicle, and time–temperature profiles of diffusion flames and adjacent structural members. The open space indicates a place where the test vehicle is in the open without re-radiated from heated surrounding, while the enclosed space denotes a place where flame behaviours are affected by surrounding structures, such as multistorey car parks and underground spaces. After determining these parameters, the next step is to theoretically/numerically predict time-dependent temperature distributions throughout spaces, loadbearing members, or local areas covered by a sprinkler system.

Since the significant LIB recall in 2006, research on the safety of LIBs has been being conducted worldwide in different levels and objectives, as summarised in Table 1. The final goal of such studies would be to reach an integrated full-interpretation of the LIB behaviour from material to product levels. As part of the goal, the purpose of this study is to understand the thermal behaviour of BEV fires by full-scale fire testing on recent BEVs with high energy capacities (i.e., Level 6). This article therefore primarily discusses the quantification of the extent of BEV fire hazards in an open-space environment for the first experimental work, as defined in the previous paragraph, to obtain the key parameters under open space and to make public the measured data for further studies.

As significant resources are expected to be required for conducting full-scale car fire experiments, such tests have been intermittently performed worldwide since the 1990 s, mostly on ICEV fires but rarely on both PHEV and BEV fires [7–16]; an analytical approach collated experimental data from several literature of large-scale car fire tests [12]. With respect to the methodologies, some works used oxygen consumption calorimetry (OCC) to physically measure the HRR of car fires [7–10,14,16]. For the measurement, the OCC includes the measurement station which measures velocity, temperature, smoke density, and concentration of combustion gas [17–18]. An early attempt to test real-scale ICEVs was made using an open OCC with a 14.2-m^2-cross-section hood and a 0.2-m^2-cross-section duct [7]. Another study connected a 9-m^2-cross-section hood with another to collect a greater quantity of the combustion products generated from ICEV fires [8]. Since the 2000 s, larger OCC was introduced to test more recently

Table 2
Specimen features and test conditions.

Features and conditions	Test 1	Test 2	Test 3	Test 4	Test 5	Test 6
	LIB pack of BEV_1	Body of BEV_1	BEV_2	BEV_3	ICEV	FCEV
Length (mm)	N/A	4,180			4,165	4,670
Width (mm)	N/A	1,800			1,800	1,860
Height (mm)	N/A	1,570			1,550	1,630
Weight (kg)	449	1,206	1,540	1,685	1,320	1,820
Nominal total energy capacity of LIB (kWh)	64.092	N/A	39.240	64.092	N/A	1.560
State of charge of LIB (%)	100	N/A	100	100	N/A	20
Thermal runaway initiation or flaming ignition	Heating a surface of single cell using a heating sheet	Heating the vehicles' bottom boundaries using a propane burner		Heating a surface of single cell using a heating sheet	Heating combustible contents of vehicles using a pan of heptane	

manufactured cars which would release greater amounts of heat once ignited [9–10,14,16]. There existed an alternative method of estimating the HRR by measuring the weight loss rate of specimens using load cells and adopting a known constant (namely the heat of combustion) in the HRR calculation [11]. This technique uses fuel consumption calorimetry (FCC) without the measurement station, thereby facilitating obtaining HRRs. However, the constant adopted needs to be firmly based on experimental data. In case of BEVs, as less information is available yet, the HRR measurement using the OCC should be preceded with the HRR calculation utilising the FCC only. In this study, both the OCC and FCC were therefore used, thereby measuring HRRs and estimating the average effective heat of combustion of BEV fires for further research.

Attempts to experiment on real-scale BEVs began to be made from the early 2010 s [12,14,16]. However, the BEVs in the previous studies were still in their infancy, which involved smaller amounts of low energy-capacity LIBs and flammable plastics than the recent models with at least 30-kWh-LIBs and luxurious interiors [19]. For up-to-date information on BEV fires, three BEVs manufactured in 2020 were experimentally examined in this study. For the first and second tests, as tabulated in Table 2, a unit of BEVs was disassembled into its body and a LIB pack. This allowed examination of individual contributions of the parts to the global BEV fire. Fires generated from two fully charged BEVs with different energy capacities were studied in the third and fourth tests. The BEV model is indistinguishable from its ICEV version as the two cars were produced from the same manufacturing platform. This ICEV version and a hydrogen fuel-cell electric vehicle (FCEV) were additionally tested in the fifth and sixth experiments to examine the thermal characteristic differences between BEV, ICEV, and FCEV. The six full-scale car fire tests were conducted upon an instrumented rig under a 10-MW-scale OCC of Korea Conformity Laboratories (KCL).

2. Experimental

2.1. Calorimetry

In fire safety engineering, the HRR and THR are critical measures enabling one to evaluate the magnitude of fire events, which are conventionally obtained from calorimeter tests based on the principle of oxygen depletion during combustion developed in the 1970–80 s [20]. These parameters for car fires have been rarely measured worldwide as the greater mass that specimens have the larger calorimetry with relevant facilities is needed. Significant laboratory, financial, technical, and manpower resources are therefore required for such tests.

In the present tests, the combustion products released from burning vehicles were collected by means of a 51.5-m^2-cross-section conical hood suspended approximately 8.6 m above the test floor, as shown in Fig. 1(a). The hood was coupled with a 3.8-m^2-cross-section exhaust duct which was connected to draft fans capable of delivering approximately 3,200 m^3/min, as shown in Fig. 1(b). As a certain amount of oxygen involved in the incoming air flow is expected to be consumed in the course of combustion of the carbon-based object (e.g., vehicles), a reduction in the oxygen concentration relative to the ambient air occurs as a function of time [21–22]. This variation is detected by a paramagnetic oxygen analyser. The changed oxygen-concentration in mole fraction was used to calculate the factor of oxygen depletion. This factor was subsequently applied to calculate the HRR and THR of tested objects, based on the fact that the average heat release per unit mass of oxygen appears to be a constant of 13.1 MJ/kg with a standard deviation of 0.35 MJ/kg [20].

2.2. Specimen

Test vehicles were the five-door models with similar dimensions and weights, except FCEV, as listed in Table 2. The BEV model was reported as developed from the identical manufacturing platform to that used for the existing ICEV version. The flame spreading behaviours in the bodies of the two types of vehicles were therefore assumed to be comparable. The BEV model had two trim-levels in terms of LIB energy capacity, which involved 39- and 64-kWh LIB packs for a normal and a long driving-ranges on one full-charge respectively, as illustrated in Fig. 2(a) and 2(b). A LIB pack was also mounted on the FCEV trunk. Its energy capacity (1.56 kWh) was much lower than those of BEVs.

The LIB packs of the drivable BEVs were fully charged in operating

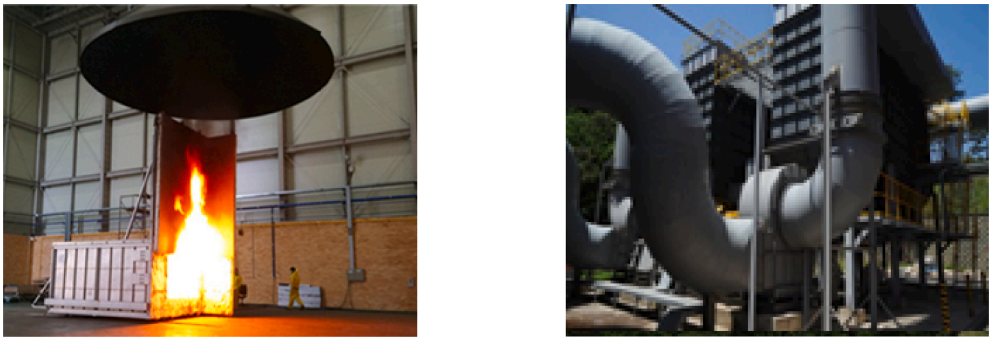

(a) A conical hood (b) Draft fans

Fig. 1. Large-scale cone calorimetry in KCL.

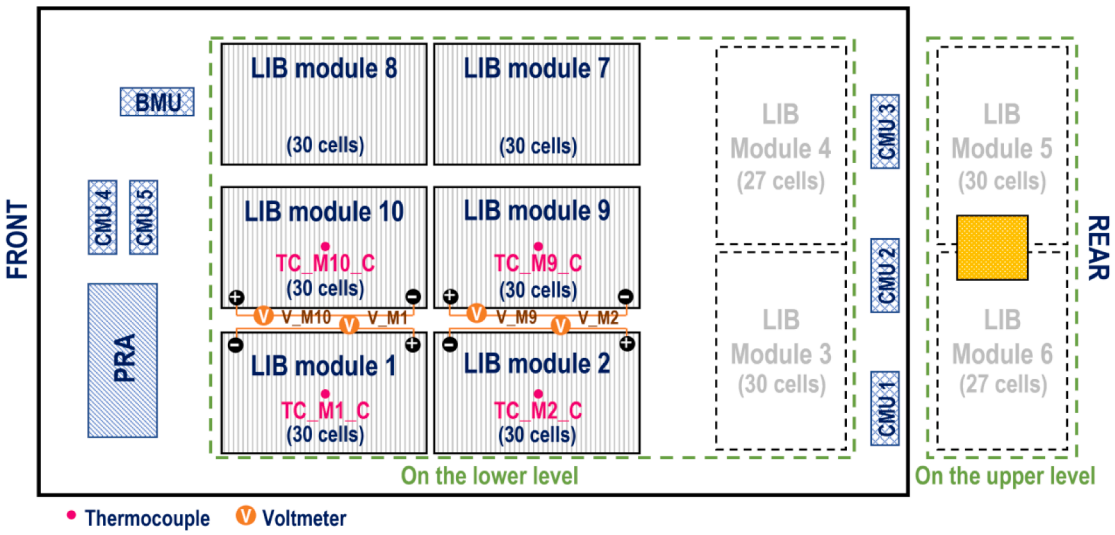

(a) 39-kWh model

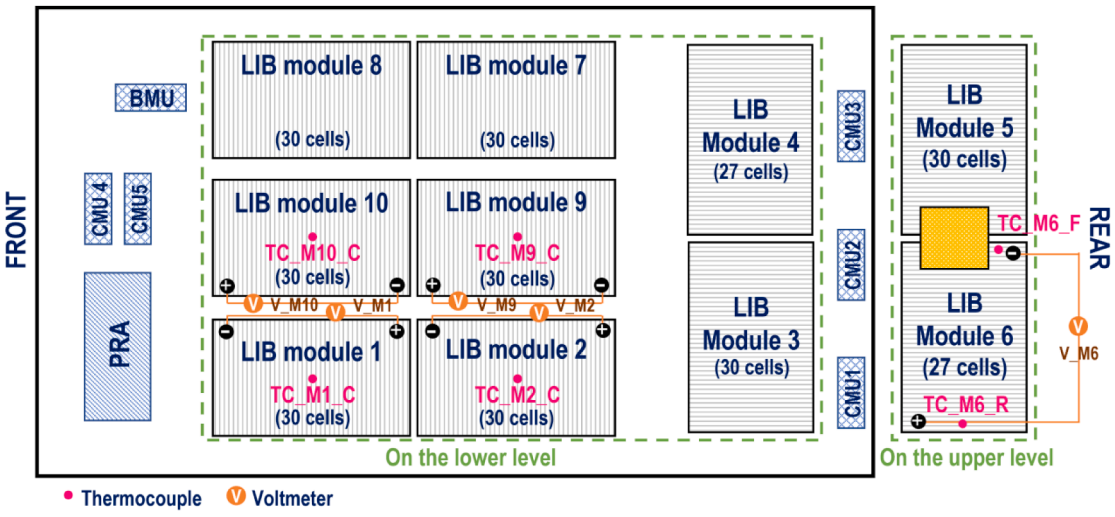

(b) 64-kWh model

Fig. 2. The layouts of LIB modules in packs with two options.

Table 3
Specifications of LIB cell.

Model	Nominal capacity (Ah)	Nominal voltage (V)	Size (mm)	Weight (g)
E63B (NCM 622)	60	3.63	(L)310×(W) 114×(t)15	887.8

conditions before disassembled from the vehicle bodies. The isolated LIB packs were subsequently opened to equip heating sheets, thermocouples, and voltmeters on the internal LIB cells, as shown in Fig. 2 and 3(a)-(c). The heating sheets were intended to initiate the thermal runaway of a predetermined cell. The thermocouples were used to examine the heat propagation from the ignited to the surrounding modules inside the packs and to the pack's metal housings. The voltmeters were used to monitor the voltage drops of modules to confirm the thermal runaway. The specifications of the pouch-type LIB cells installed in the BEVs are listed in Table 3. Fig. 3(d) shows the distribution of thermocouples in the passenger cabin, motor compartment, trunk, and tyres. For the third and fourth tests, the instrumented LIB-packs and BEV-bodies were reassembled. Although the reassembled BEVs were operatable, the specimens were moved upwards and away by a forklift truck for safety purposes as the BEVs' cooling system was disconnected. After the preparations, all the specimens were covered with waterproof polyvinyl chloride (PVC) blankets and conditioned indoors for at least 2 weeks before the experiments.

2.3. Instrumented test rig

To facilitate the measurement of multiple parameters during the large-scale fire testing, a test rig was designed. The rig was composed of a mounting platform, structural steel members (columns and beams), and one-way water-cooled pipes, as shown in Fig. 4(a). As it was expected that fire plumes with high temperature over 800 ℃ would maintain for at least 10 min during each of the tests, tap water at room temperature was allowed to flow through the ceiling and column pipes of the rig to prevent its thermal failure. The rig dimensions were determined based on the Korean regulations for the minimum size of a standard parking space with a 2.5 m width, a 5.0 m length, and a 2.3 m

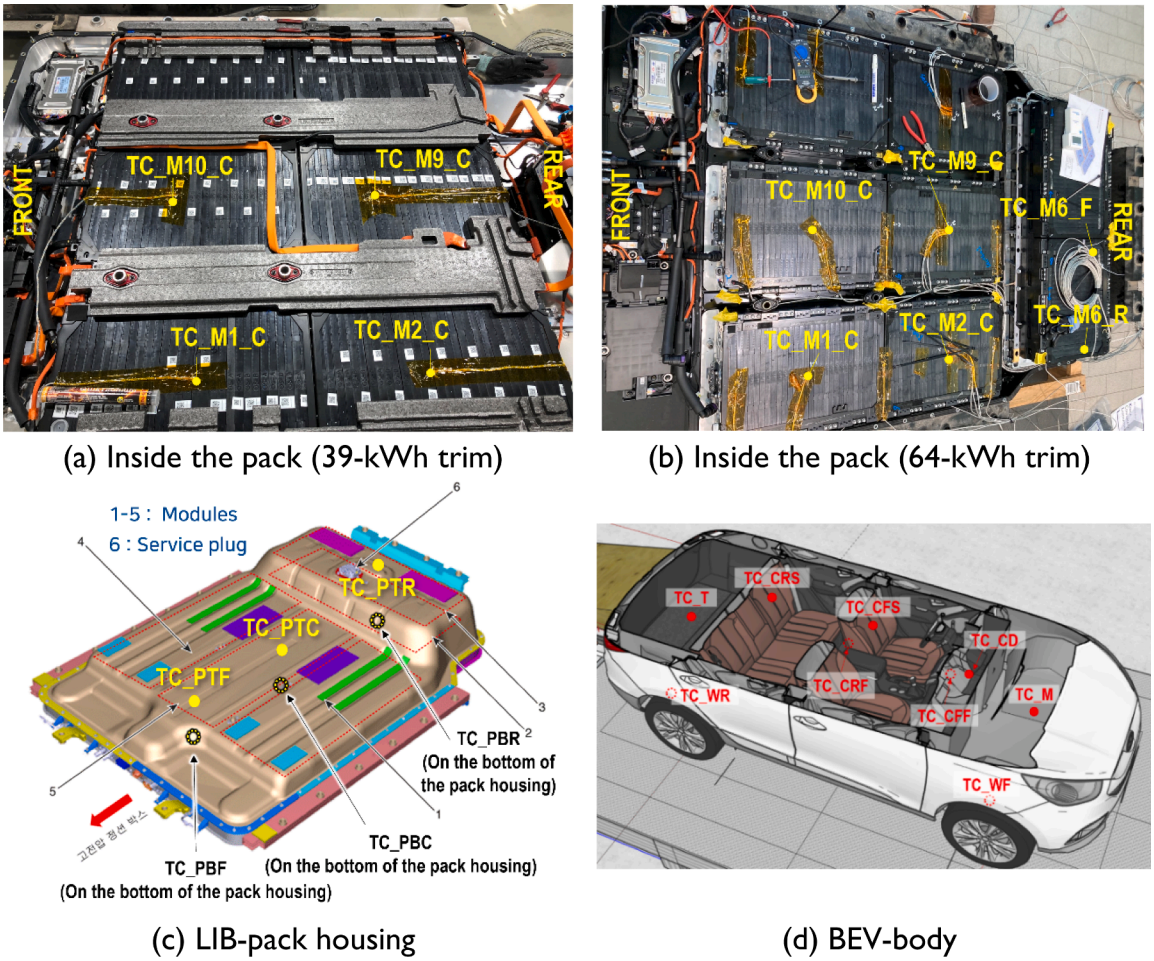

Fig. 3. Instrumented LIB packs.

height. Three types of sensors were installed in the rig, which were the thermocouple, heat flux gauge, and load cell, as illustrated in Fig. 4:

- To measure the temperature of combustion gas above different parts of the vehicle, thermocouples (Model: 24-AWG k-type dual-wall insulated wire) were aligned with the vehicle's longitudinal mid-plane on the upper water-cooled pipes (TC_GB, TC_GW, TC_GR, and TC_GCRW), as illustrated in Fig. 4(b). Thermocouples were also positioned at the mid-height of the vehicle's front- and rear-seat windows (TC_FW and TC_RW at $z = 1{,}270$ mm) and at the same x- and y-coordinates but on the upper pipes (TC_GFW and TC_GRW at $z = 2{,}270$ mm);
- Four water-cooled Schmidt-Boelter gauges (Model: SBG01, Hukseflux) were aligned with the rig edges at $z = 1{,}270$ mm, facing the front-bonnet, trunk, left front- and rear-seat windows of vehicles. These positions were intended to estimate the amount of irradiance on a vehicle parked adjacent to a burning BEV;
- Four load cells composed of 16 strain gauge transducers that range from 0.5 to 1,000 kg each (Model: R-1000, CAS) were assembled with the mounting platform. The sensors measured the variation in mass of the specimen during the combustion of vehicles.

All time-dependent data of temperature, heat flux, and weight were acquired at intervals of 0.1 s using a DAQ system (Model: CompactDAQ, National Instruments). Finally, the specimen was surrounded by eight video cameras to observe its thermal behaviour and fire events.

2.4. Procedure

A series of instrumented specimens were placed at the centre of the mounting platform in order. For smooth combustion, the front- and rear-seat windows of vehicles' left doors were half-opened to allow air flow in to the passenger cabin, wherein the front, rear, left and right indicate the ordinary directions of driving. Air in the tyres was deliberately released so as to prevent unnecessary explosions. The thermal runaway of LIB packs was initiated by either heating a single LIB-cell inside the pack or heating the lower boundaries of the pack, as listed in Table 2:

- A 575-W heating sheet with 90 × 65 mm in dimensions was taped to the surface of a mid-cell of the LIB-pack's central module (i.e., Module_9), as demonstrated in Fig. 5(a). The heater was powered by an electric power supply enabling one to manually control voltage and current. A constant amount of electrical energy was intended to be consistently supplied to the heater. Once thermal runaway was triggered, the electricity was cut-off due to the electrical short-circuit failure of the heating element. This setup was intended to simulate a typical scenario of thermal runaway originating from abuses or defects in the LIB cell inside the pack;
- A 300-kW sand-box burner supplied with propane was placed underneath the LIB pack, as illustrated in Fig. 5(b), which was planned to simulate a worst-case scenario of car accidents in which a quantity of fuel has spilled, spread, and ignited underneath a BEV.

The experiments aimed to collect physical quantities in the condition of the BEV combustion. The test setup therefore focused on triggering a

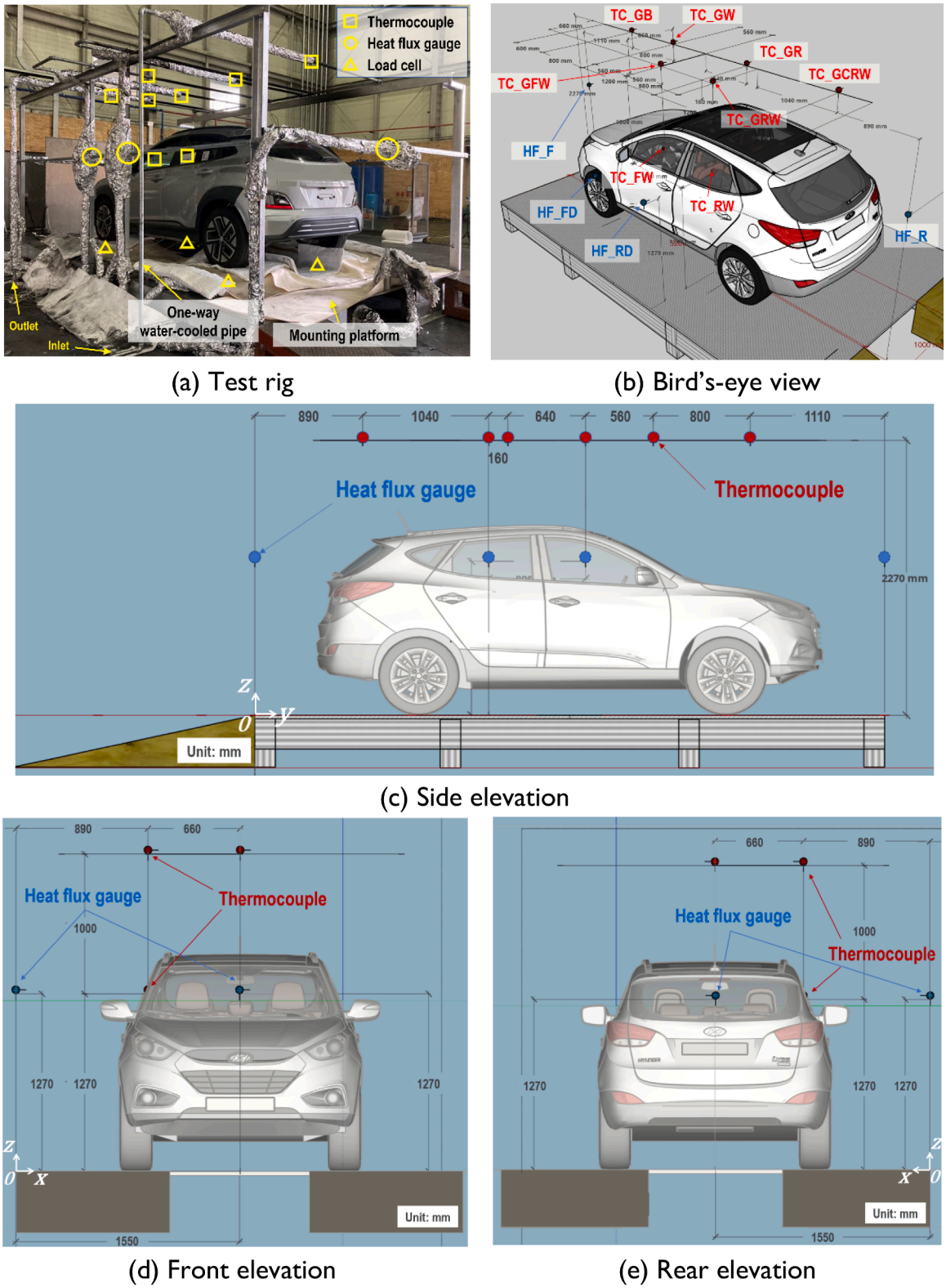

Fig. 4. Location of sensors in the testing rig.

thermal runaway rather than on examining the parameters representing a thermal runaway initiation or a flaming ignition, such as the activation energy of thermal runaway, and the time to the onset of the phenomenon. All specimens were allowed to be fully burnt out during the tests.

3. Results and discussion

3.1. HRR and THR of car fires

Fig. 6 shows the overall HRR and THR profiles in the six tests, physically measured in the open-space condition using the large-scale

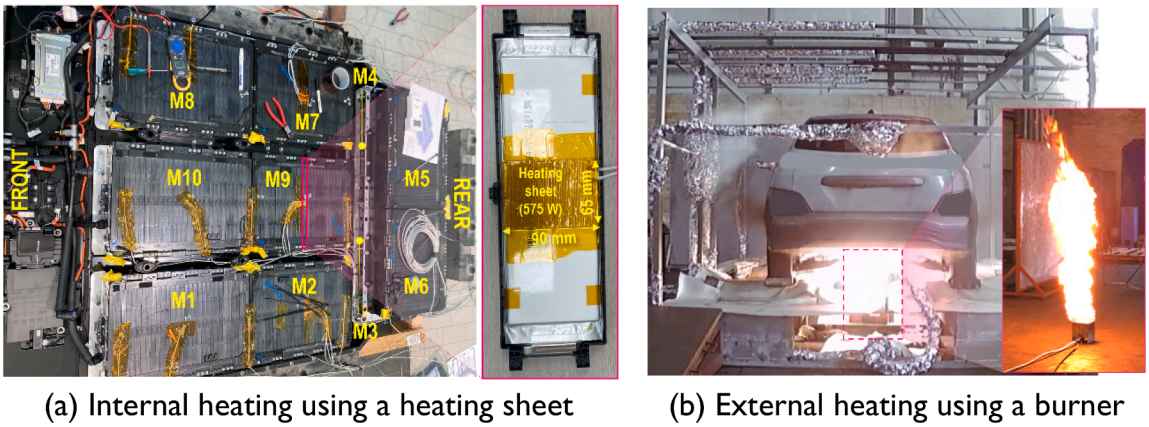

Fig. 5. Initiation of thermal runaway.

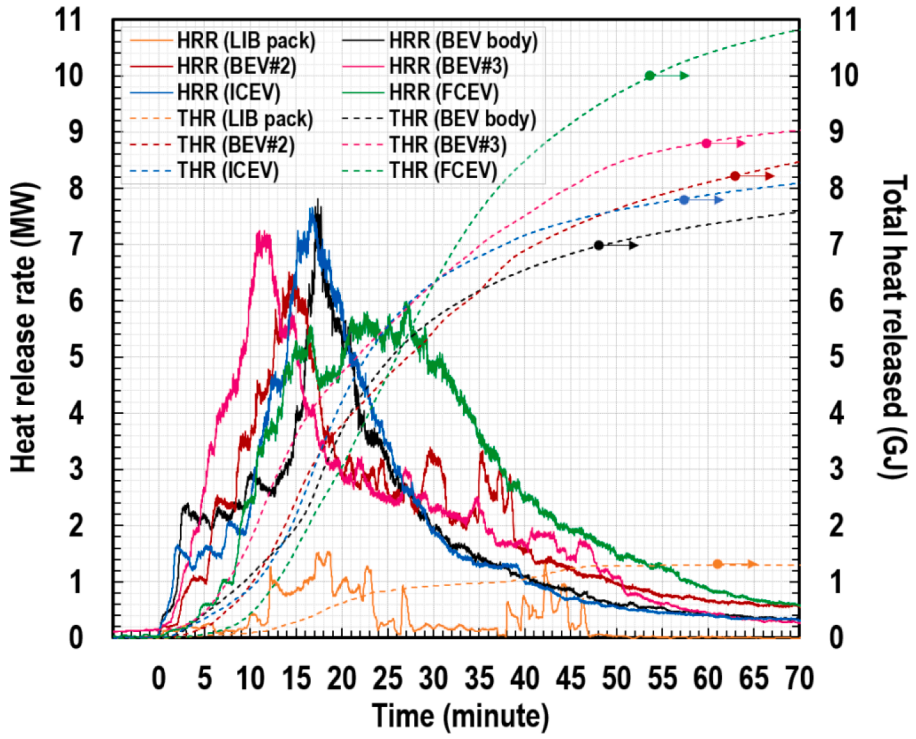

Fig. 6. Time-dependent profiles of HRR and THR.

Table 4
Measures of thermal hazards of vehicle fires.

Measures	Test 1 LIB pack of BEV_1	Test 2 Body of BEV_1	Test 3 BEV_2	Test 4 BEV_3	Test 5 ICEV	Test 6 FCEV
Peak heat release rate, pHRR (MW)	1.54	7.81	6.51	7.25	7.66	5.99
Total heat released, THR (GJ)	1.30	7.53	8.45	9.03	8.08	10.82

cone calorimetry. The solid and dashed lines denote the HRR on the scale of the primary vertical axis and the THR on that of the secondary vertical axis, respectively. In the figure, to facilitate the comparison among the data, all the onsets of HRR growths were adjusted at zero min. Overall, personal vehicle fires remained for at least 70 min until the full burnt-out in the open-space environment. In the very early stage of fires (approximately 1–2 min), the rapid increases in HRR were observed in the BEV-body, BEV_2, and ICEV tests. These prompt growths were caused by the activation of the ignition tools (i.e., the propane burner or heptane pans, as introduced in Table 2), rather than any rapid combustions of the specimens. In the fire growth stage, the ignited vehicles generated gradually-increasing heats and reached peak values (i.e., pHRR) in approximately 11–17 mins. The fully developed fire stages during the tests, were not maintained for a long period, except the FCEV. The fires subsequently turned into the fire decay stage with gradual decreases in HRR. In this stage, fluctuations in HRR were observed in the BEV_2 and BEV_3 tests due to a series of thermal runaway events. The HRR and THR of the LIB pack were smaller than those of the vehicles, and fluctuations were also observed due to the thermal runaway phenomena.

The HRRs and THRs of all the specimens are tabulated in Table 4. The parts of the HRRs produced from the ignition burner or fuel pans were excluded in the THR calculation. The LIB pack (64 kWh) and BEV-

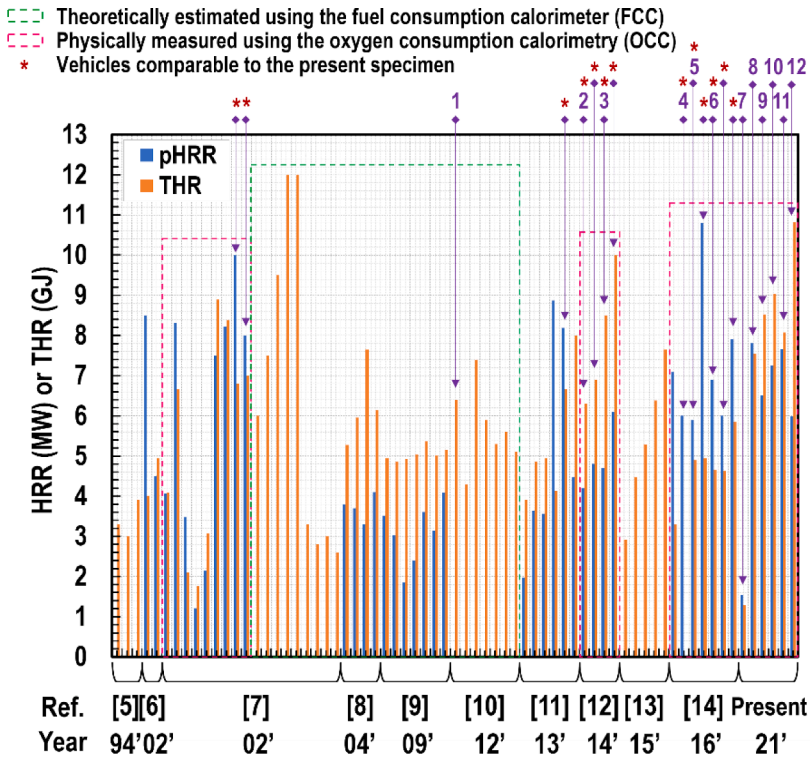

No.	Model or type / Energy capacity	Initial mass (kg)
1	Nissan leaf / 24 kWh	1,520
2	BEV / 16.5 kWh	1,112
3	BEV / 23.5 kWh	1,501
4	BEV / N.A	1,448
5	BEV / N.A	1,475
6	BEV / N.A	1,650
7	LIB pack / 64 kWh	449
8	BEV-body / N.A	1,206
9	BEV / 39.2 kWh	1,540
10	BEV / 64.1 kWh	1,685
11	ICEV / N.A	1,320
12	FCEV / 1.6 kWh	1,820

Fig. 7. Chronological data of pHRR and THR for vehicle fires.

Table 5
Categories of *t*-square fires [23].

Growth rate	t_1 (s)	θ(MW/s^2)	Typical real fires
Slow	600	0.0028	Densely packed wood products
Medium	300	0.0111	Solid wood furniture (desks), or individual furniture items with small amounts of plastic
Fast	150	0.0444	High stacked wood pallets, cartons on pallets, or some upholstered furniture
Ultrafast	75	0.1778	Upholstered furniture, high stacked plastic materials, or thin wood furniture (wardrobes)

body fires generated 1.54 and 7.81 MW of pHRR and 1.30 and 7.53 GJ of THR, respectively. The BEV_3 with the 64-kWh pack resulted in heat with 7.25 MW of pHRR and 9.03 GJ of THR, respectively. The THR of the BEV_3 fire was comparable with the sum of the individual THRs of the pack and body (8.83 GJ). This observation led to a summary that a larger contribution of BEV fires came from the BEV-body than the LIB-pack in terms of pHRR and THR. Accordingly, the combustion that occurred in the passenger cabin governed the two measures in the BEV fires, despite the vigorous thermal runaway generated from the LIB packs. This is based on the presumption that greater amounts of combustible materials exist in the body, particularly in the cabin, than in the pack. The initial weights of the vehicle-body and pack were 1,206 and 449 kg, respectively. Although no information on such amounts were available, the proportions of the combustible materials used in the body and pack could be estimated by measuring the amounts of mass lost after full combustions, which are discussed in the following sections.

A gap existed between the THR values for the BEV_2 and BEV_3 fires due to the difference between the energy capacities of the two vehicles. The THRs of the BEV fires were higher than that of the ICEV but smaller than that of the FCEV. This tendency was parallel to their weights. It should be note that such comparative works are acceptable with respect to THR but not as regards pHRR. The pHRR represents a phenomenon of burning at the limited instant at which the most volatiles are simultaneously combusted. In the extent of vehicle fires, as the simultaneous combustions generally depends on several aspects, such as the location of ignition spot, order of flame spread, and ventilation condition, it is challenging to find a correlation between the pHRR and weight.

Fig. 7 shows the chronological data of pHRR and THR for the vehicle fires in the existing studies [7–16] and present paper. The pink and green dashed boxes indicate the respective data that were physically measured using the OCC and that theoretically estimated using an average effective heat of combustion with the measured mass loss rate utilising the FCC. There is a lack of information on the rest. Most of the data are associated with ICEV fires, while a few papers demonstrate the parameters for BEV fires as pointed out with the numbers in the figure and tabulated in the legend table, except No. 7, 11 and 12; the asterisk denotes the vehicles comparable to the present specimen in terms of the size and curb weight. From the data, summaries can be made, as follows: (1) The present measurements remained in the pHRR and THR ranges for the models with the asterisks. (2) The data for the recent BEV model (No. 9 and 10) were greater than those for the earlier models (No. 1–6) due to the comparatively large quantities in BEV mass and LIB energy capacity. (3) It was challenging to generalise about the tendencies on the pHRR and THR along year or mass for the extent of car fires due to the differences in car-model, -size, the materials applied, and the HRR measurement method.

3.2. The degree of fire growth

The degrees of the BEV fire growth were quantified adopting a generic fire-growth curve (i.e., *t*-square fire) used in fire protection analyses. A growth of the time-dependent HRR can be characterised by the time to reach 1 MW of HRR (t_1 in s), which is generally categorised into four levels based on the growths of typical real fires, as listed in Table 5. The relationships among HRR ($\dot{Q}_f$), t_1, and time (t) are defined as follows [23]:

$$\dot{Q}_f = 1,000(t/t_1)^2 = \theta t^2 \quad (1)$$

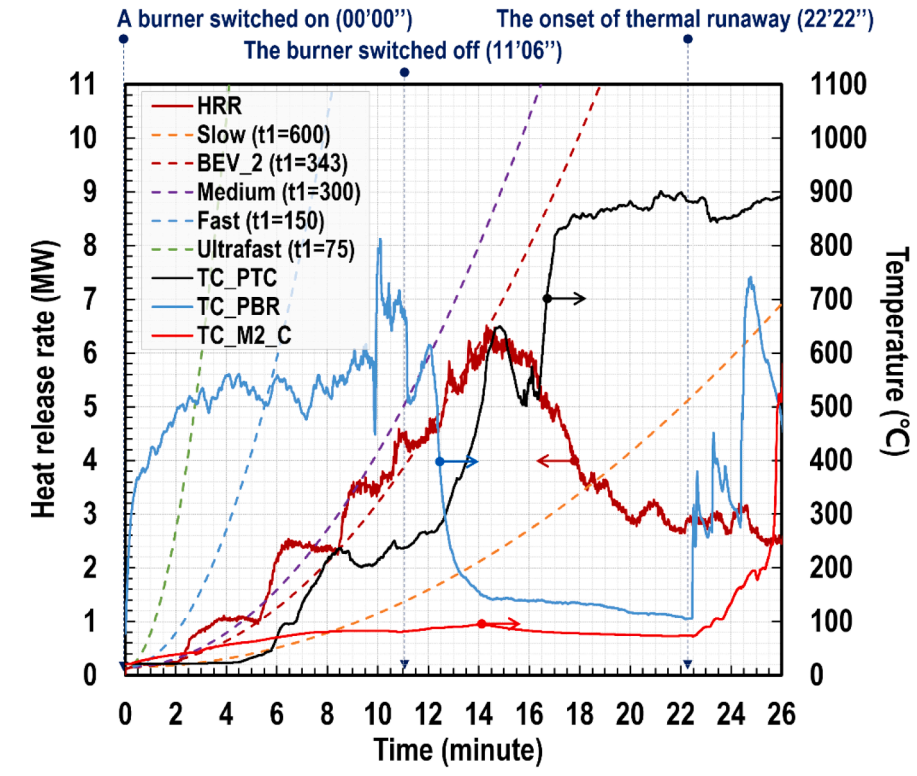

(a) BEV_2 in Test 3

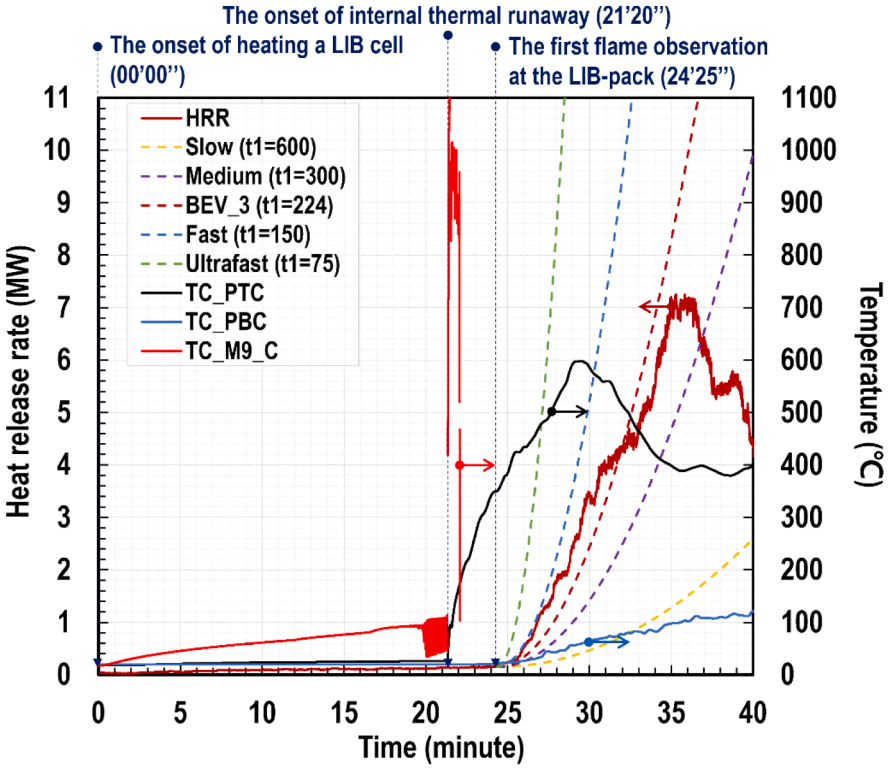

(b) BEV_3 in Test 4

Fig. 8. The quantification of BEV fire growths in Tests 3 and 4.

where θ denotes the parameter of growth.

Fig. 8(a) and (b) show the changes in the HRR at the fire growth stage in the third and fourth tests, respectively, with design fire scenarios; dashed lines denote the calculated *t*-square curves with the typical growth rates listed in Table 5. The time–temperature profiles demonstrate the temperature variations of the LIB packs at the same stage (i.e., TC_PTC, TC_PBR, TC_PBC, TC_M2_C and TC_M9_C, as illustrated in Figs. 2 and 3(c)). Important events are described on the top of the figures

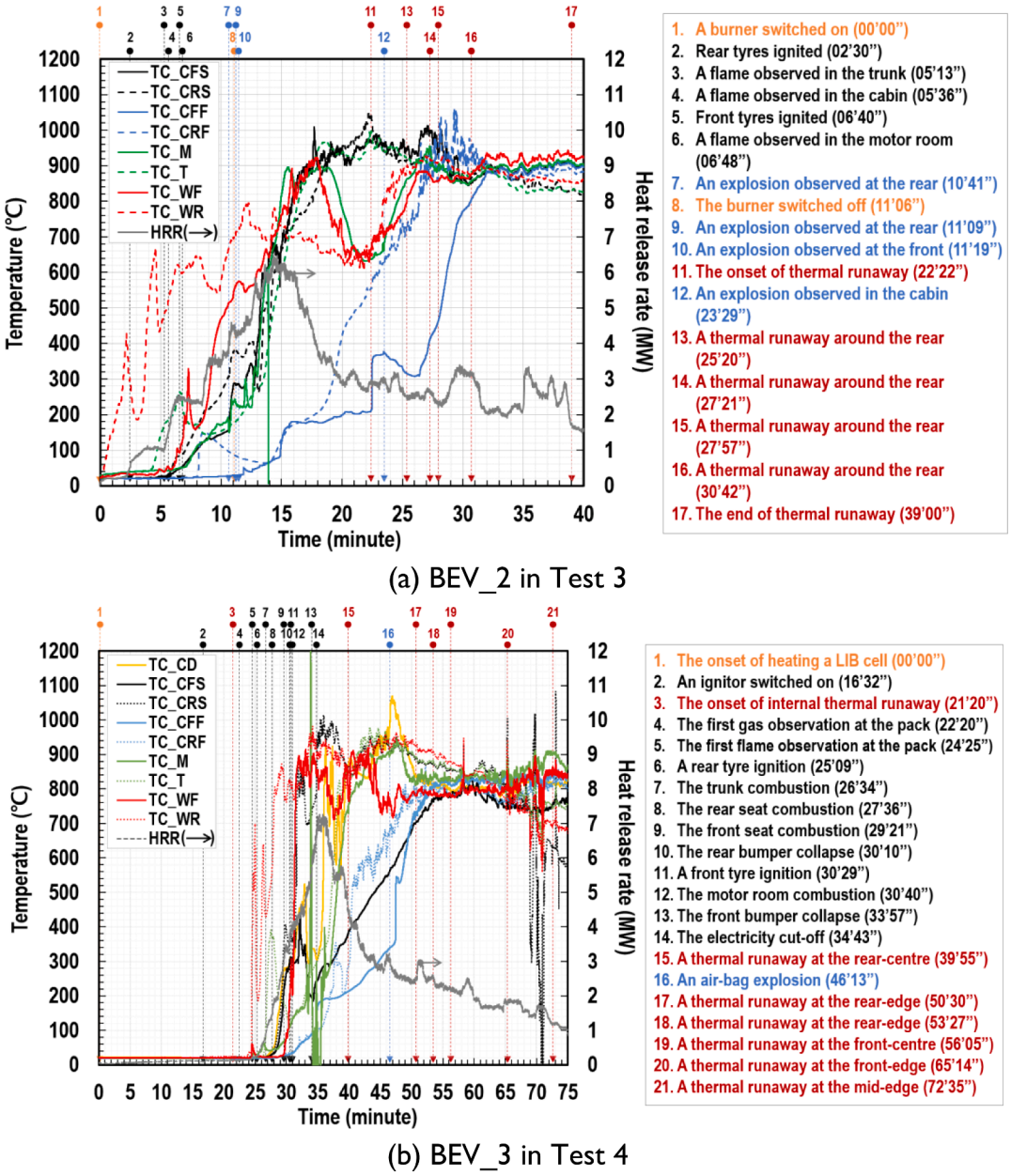

Fig. 9. Temperature-time profiles of BEVs in Tests 3 and 4.

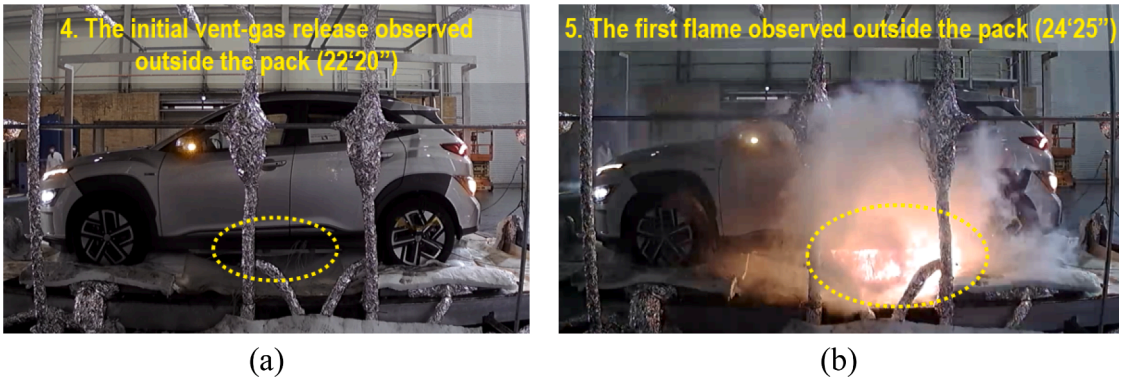

Fig. 10. Photos of the specimen status at the important events in Test 4.

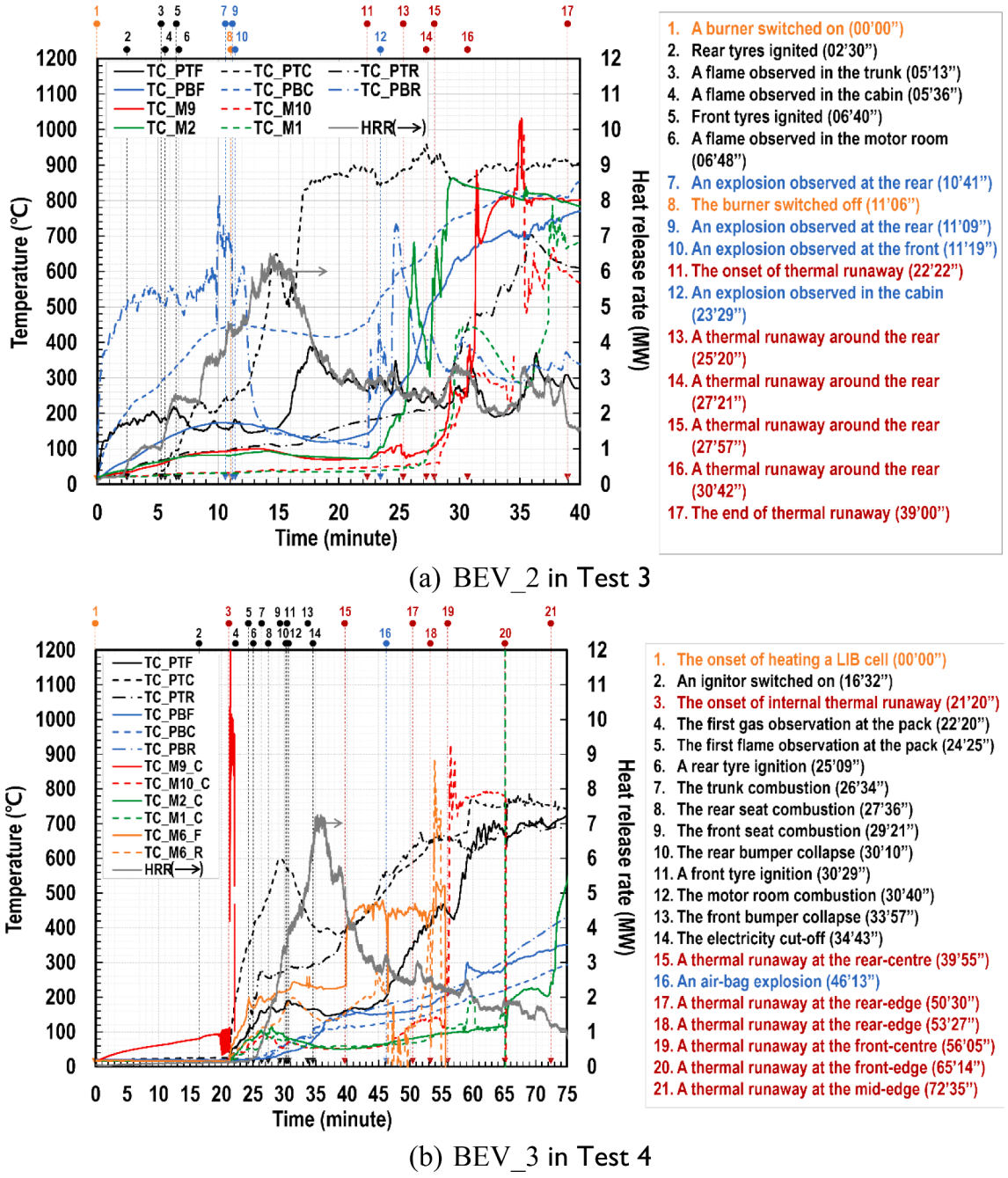

Fig. 11. Time-temperature profiles of LIB-packs.

with arrows marking the temporal points at which these incidents occurred during the tests. Note that as explained in the previous section of procedure, two different heating methods were applied in the third and fourth tests; thus, the temporal points at which the HRR started rising were not identical in the two tests.

The growth parameters (θ) for the BEV_2 and BEV_3 fires were estimated to be 0.0085 and 0.020 respectively by plotting best-fit curves to the measurements, as expressed with crimson dashed lines in Fig. 8(a) and 8(b). The quantities indicate that these fires developed with the rates reaching 1 MW of HRR approximately 343 and 224 s after their ignitions, respectively. These rates can be qualified by 'slow medium' and 'fast medium', respectively, based on the categories in Table 5. Particularly, the BEV_3 fire exhibited a faster rate than BEV_2, as well as the swiftest rise to the peak over other test vehicles as shown in Fig. 5, even though the two cars were identical BEV models, with the exception of the energy capacities of the LIB packs. The difference in the growth rate between the two car fires is closely related with the difference in the major source spreading flames to adjacent combustible materials. The jet flame discharging from the BEV_3 LIB pack heated neighbouring components more vigorously than the 300-kW-burner did in the BEV_2 fire.

In the BEV_2 test, the 300-kW-burner continuously heated the bottom of the LIB pack for 11 min and 6 s, as evidenced by the blue solid line in Fig. 8(a). This heating approach resulted in a rapid increase in the pack housing (TC_PTC and PBC) and early ignitions of tyres (TC_WF and WR), as shown in Fig. 8(a) and 9(a). Although the ignited flames were subsequently spread to the trunk and cabin in order, the flame spread failed to trigger any thermal runaway of LIB modules until the pHRR at approximately 15 min, as shown in Fig. 8(a); the first thermal runaway of modules was observed at 22 min and 22 s (TC_M2_C). On the other

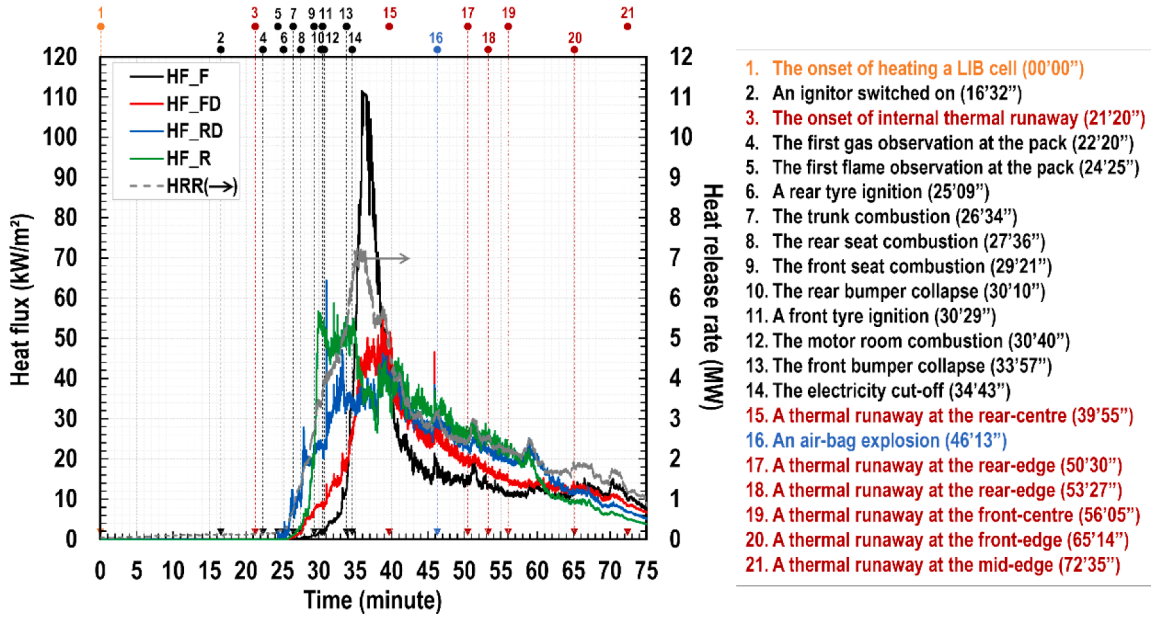

(a) BEV_3 in Test 4

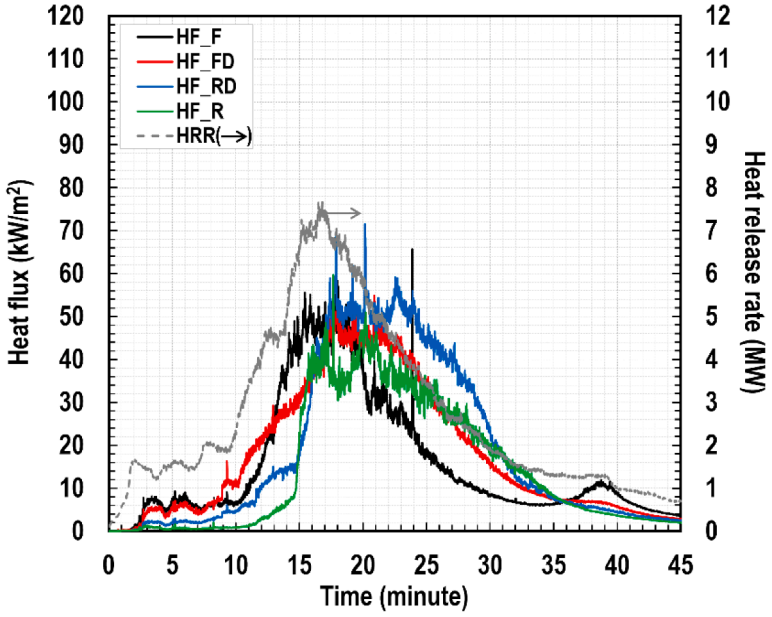

(b) ICEV in Test 5

Fig. 12. The time-dependent heat flux variations in BEV_3 and ICEV fires.

hand, in the case of BEV_3, a mid-cell in the central LIB module in the pack (M9) was heated by an electric heating sheet until the onset of the first thermal runaway at 21 min and 20 s, as shown with the red solid line (TC_M9_C) in Fig. 8(b). As this heating approach raised a local temperature inside the pack-housing, other components of the car had maintained the ambient temperature until the onset of thermal runaway, as illustrated in Fig. 9(b). The list on the right of the figures indicates the critical events observed during tests; the moments in time for these events are marked with numbered arrows in the graphs. Once triggered, grey vent-gas and jet flames were sequentially emitted, as shown in Fig. 10(a) and 10(b), respectively; the photos captured at each of the events are shown in Figs. A1 and A2. These flames heated the rear tyres and other components vigorously, which resulted in rapid spreading to the passenger cabin in which many combustibles of the car-components existed in the condition of ambient temperature.

From the observation on the measurements, several findings can be summarised, as follows: (1) The jet flame released from the LIB pack led to the rapid growth of the BEV fire. (2) Although the jet fire originating from the LIB pack accelerated the ignition and combustion of other BEV components, the jet flame was not the primary contributing factor to the HRR and THR. Rather, the majority of the heat released at an instant (i.e., pHRR) was governed by the flames created from the conventional combustion of the organic-polymer components of the car. (3) The BEV fire originating from the LIB pack was more rapidly developed than that derived from elsewhere, as well as that in the ICEV and FCEV fires as evidenced in Fig. 6. (4) The first responders should be more cautious when approaching an accident site of BEVs. This is because the damage of LIBs inside the pack housing is unobservable from outside the vehicle and the activation of thermal runaway is unpredictable. In addition, once triggered the fire is rapidly developed.

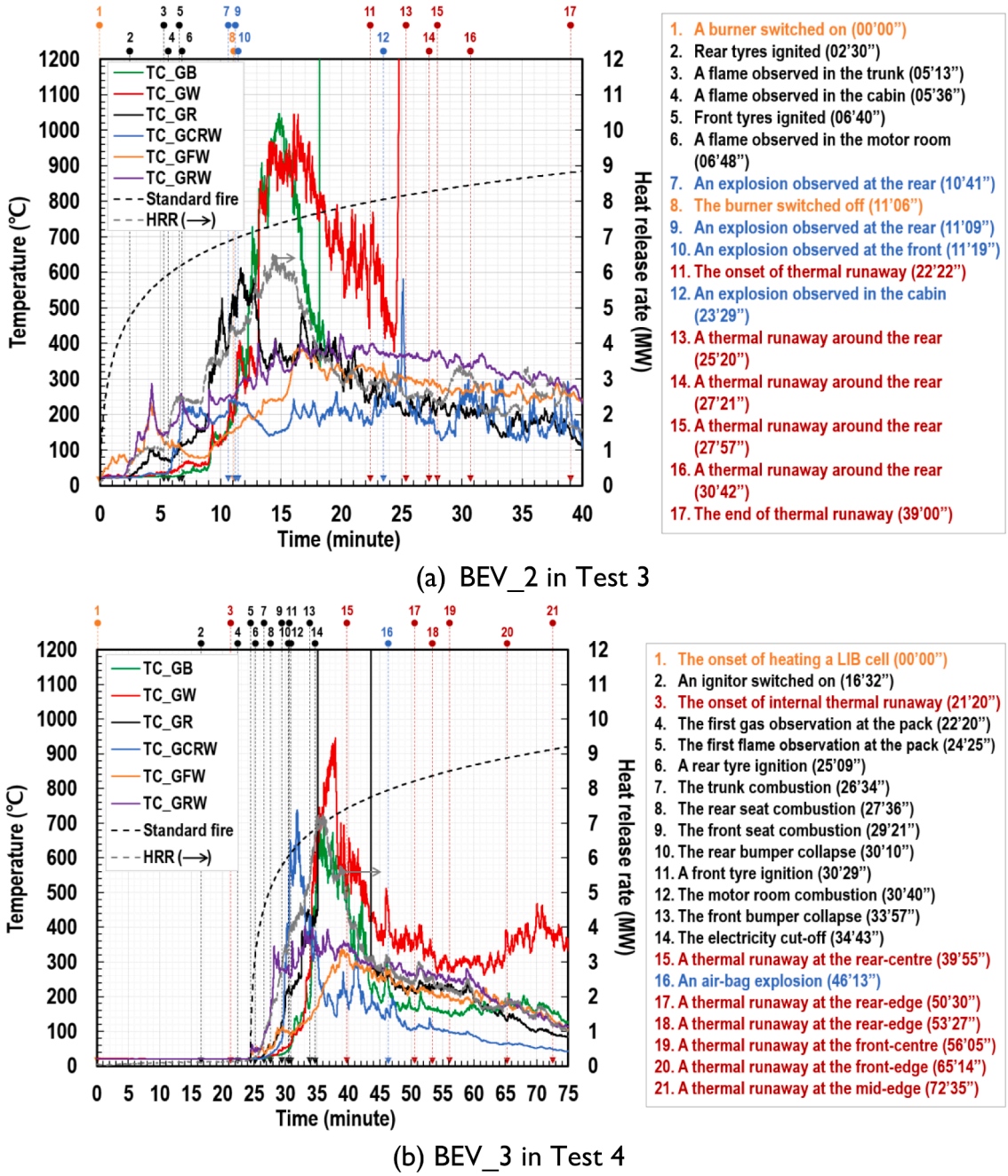

Fig. 13. The time–temperature profiles of fire plumes in BEV_2 and BEV_3 fires.

3.3. Observation of LIB-pack temperatures

Fig. 11(a) and 11(b) show the time-dependent temperature variations inside and outside the LIB packs of BEV_2 and BEV_3, respectively. The thermocouples locations in the legend are described in Fig. 2. In the BEV_2 test, the external heat source initially raised the surface temperature of the lower alloy-housing (TC_PBF, PBC and PBR). Although heat was transferred through the metal to the housing's upper area (TC_PTF, PTC and PTR) in conduction, it is likely that the temperature rise of the upper part was mainly caused by the heat generated from the flames spread to the tyres and passenger cabin. The first thermal runaway was identified at the eleventh event, which was approximately 7 min after the HRR peak (pHRR). Since then, a series of thermal runaways occurred in the LIB modules at M2, M1, M9, and M10 in order, which resulted in the rapid temperature rise of the metal-housing with a high heat capacity, up to approximately 800 °C. In the BEV_3 test, the thermal energy generated from the first thermal runaway of the nineth module directly contributed to the temperature rise in the upper housing from the pack inside, due to the buoyancy of hot vent-gas and flames. Thermal runaway was extended at M9_C, M6_F, M6_C, M10_C, M1_C, and M2_C in order. The lower area temperature of the housing was gradually increased.

From the heat transfer viewpoint, the external heat originating from the propane burner underneath the LIB pack is supposed to be distributed to the alloy-metal housing, internal LIBs, BEV body frame, and surroundings. The amount of thermal energy transferring to the LIBs could be reduced, provided that a large quantity of heat is dissipated to the others. The metal housing that directly faces the external flame has a relatively high heat inertia. This mass absorbed a certain amount of thermal energy to raise its temperature, thereby retarding the increase in

Table 6
Gross combustion efficiency of vehicles.

Specimen, year	m_{ini}[kg]	m_{end}[kg]	$\Delta m/m_{ini}$[%]	$\Delta H_{c,eff}$[MJ/kg]
ICEV(Peugeot 406), 2002 [9]	1,454	1,192	18.0	26.0
ICEV(Peugeot 406), 2002 [9]	1,362	1,107	18.7	27.5
ICEV(C2), 2013 [13]	1,303	1,029	21.0	24.4
BEV(SOC100), 2014 [16]	1,448	1,115	23.0	N.A
BEV(SOC85), 2014 [16]	1,475	1,180	20.0	16.6
ICEV, 2014 [16]	1,344	1,008	25.0	14.7
BEV(SOC100), 2014 [16]	1,650	1,287	22.0	12.8
PHEV(SOC85), 2014 [16]	1,467	1,159	21.0	15.0
PHEV(SOC100), 2014 [16]	1,712	1,267	26.0	13.1
LIB pack, 2020–2021 [Present]	449	421	6.3	45.9
BEV body, 2020–2021 [Present]	1,206	944	21.7	28.8
BEV_2, 2020–2021 [Present]	1,540	1,256	18.4	29.8
BEV_3, 2020–2021 [Present]	1,685	1,389	17.6	30.5
ICEV, 2020–2021 [Present]	1,320	1,026	22.3	27.4
FCEV, 2020–2021 [Present]	1,820	1,423	21.8	27.3

the internal LIB temperature. It was observed in Fig. 11(a) that the temperatures of the thermocouples positioned on the exposed bottom-surface of the housing (i.e., TC_PBF, PBC, and PBR) increased rapidly in the direct heating condition, while the temperature increases of the LIB modules (i.e., TC_M_1, 2, 9 and 10) were relatively slow. It is well known that the alloy-metal material allows heat to rapidly transfer to the internal components due to its high thermal conductivity. It was additionally realised that this massive solid partially contributed to the thermal protection of the internal LIBs against external heating for a limited period of time by absorbing heat. On the other way, it could be challenging to lose heat from the alloy cover and to prevent the temperature increases of internal LIBs once this mass reaches a threshold temperature.

3.4. Thermal hazard to adjacent objects

Fig. 12(a) and 12(b) show the time-dependent variation in total exposure heat fluxes arriving at the predetermined four points surrounding and distanced from the burning cars in the fourth and fifth tests. Both the car fires recorded their peaks at the points mostly within a range of 40 to 60 kW/m^2 in the fully developed fire stage. Although one of the values exceptionally reached up to 110 kW/m^2 at the BEV front, more tests should be repeated to justify this phenomenon. In further studies, the exposure heat fluxes measured at the points using heat flux gauges ($\dot{q}''_g$) could be used to evaluate the possibility of an adjacent car ignition by predicting the car's surface-temperature (T_s). The incident heat flux on the measuring area of the gauge ($\dot{Q}_g$) is equal to the heat released from the fire source ($\dot{Q}_f$) multiplied by the absorptivity of the probe's surface (α_g) and the configuration factor from the fire to the gauge (F_{f-g}), as follows:

$$\dot{Q}_g = \alpha_g F_{f-g} \dot{Q}_f \tag{2}$$

The dash in the subscript of F implies "to". The thermal energy, $\dot{Q}_f$, has a relationship with the measured heat flux, $\dot{q}''_g$, as follow:

$$\dot{Q}_f = \frac{A_f}{\alpha_g F_{g-f}} \dot{q}''_g \tag{3}$$

where $F_{f-g} = A_g/A_f F_{g-f}$. Accordingly, the time-dependent surface-temperature development, $T_s(t)$, can be obtained using the global conservation equation for energy, as follows:

$$\rho_s c_{p,s} V_s \frac{dT_s}{dt} = A_s \left[\frac{\alpha_s}{\alpha_g} \dot{q}''_g - \varepsilon_s \sigma \left(T_s^4 - T_\infty^4 \right) + h_s \left(T_f - T_s \right) \right] \tag{4}$$

Fig. 13(a) and 13(b) show the time–temperature profiles of buoyant fire plumes measured at a 2,270-mm height and generated from BEV_2 and BEV_3, respectively. The two fires resulted in peak temperatures beyond 900 ℃ which were mainly contained contributions from the fire plumes above the bonnet and front window of the cars (TC_GB and GW). The peak moments of the HRRs were similar to those of the temperatures in the tests. The black dashed line in the figures indicates a nominal temperature–time curve based on the early tests in the 1900 s, which has been most widely used in building fire engineering [24]. The BEV fires are likely to endanger the durability of the structural members above the cars for at least 10 min, in which the gas temperatures exceeded that of the standard fire curve. In the BEV_3 case, its combustion is expected to be more hazardous to the structural members than that of BEV_2, due to its rapid growth and intensive heat released.

The concept of average effective heat of combustion ($\Delta H_{c,eff}$ in MJ/kg) that represents the gross combustion efficiency of a substance was adopted to evaluate the present BEV fire hazards. This approach could generate date for further studies on the safety measures. The parameter for the fire generated from the BEV combustion was defined to be a constant from the engineering application viewpoint, as follows:

$$\Delta H_{c,eff} = \int_{t_{ini}}^{t_{end}} \frac{\dot{Q}_f(t)}{\dot{m}_{loss}(t)} = \frac{THR}{m_{ini} - m_{end}} \tag{5}$$

Table 6 shows the calorific values, $\Delta H_{c,eff}$, and the relevant mass measurements of the previous and present specimens; the prior samples were introduced with asterisks in Fig. 7. As a result, mass in the range of 17.6 to 26 % of the total weight was generally burnt during car fires. Approximately 30 MJ/kg of $\Delta H_{c,eff}$ was recorded from the present BEV fires, which was greater than the values for the ICEV and FCEV fires, as well as for the individual combustion of the BEV-body. This was because the total heat generated from the LIB pack (1.3 GJ) was relatively large as compared to the amount of mass consumed (28 kg). The overall heat intensity released per unit mass therefore increased in the BEV fires. For the individual LIB pack, $\Delta H_{c,eff}$ was estimated to be 45.9 MJ/kg, which was comparable with those of flammable fuels and highly combustible polymers, such as *n*-Pentane (45.69 MJ/kg [25]) and polypropylene (42.66 MJ/kg [26]). This finding is related to the fact that major flammable components of a LIB cell are typically polypropylene and polyethylene (44.60 MJ/kg [26]) for separators and mixed carbonate solvents (12.7–24.7 MJ/kg [27]) for electrolytes. Additionally, it turned out that the $\Delta H_{c,eff}$ calculation was highly dependent on the applied test methods for measuring the HRR and relevant test environments, which made the generalisation of a correlation between mass and $\Delta H_{c,eff}$ challenging.

4. Conclusions

To quantitatively evaluate the hazards caused by battery electric vehicle (BEV) fires, a series of real-scale fire tests were conducted on the BEVs and the separated parts of lithium-ion battery (LIB) pack and BEV-body. Other types of cars, such as internal combustion engine vehicle (ICEV) and hydrogen fuel cell electric vehicle (FCEV) were additionally tested for comparative purposes.

Although several full-scale car-fire tests have been performed in prior studies, limited studies focused on BEVs. Existing literature is for early BEV models. In markets, personal hybrid vehicles have been shifting to be larger and more luxurious, and have larger energy capacity of LIBs in case of BEVs. To cope with this trend, an innovative test scheme was designed on the instrumented test rig under the 10-MW calorimeter system. Thermocouples were additionally installed inside

Fig. A1. Photos of the specimen status at the critical events in Test 3.

the LIB packs to observe the heat progress among internal LIB modules. To initiate the thermal runaway of LIBs, internal and external heating methods were employed by using the heating sheet and 300-kW-propane-burner, respectively. These setups represent a typical scenario of thermal runaway accidents and a worst-case scenario of fuel-spilled car accidents, respectively.

All the specimens were burnt out completely under the calorimetry hood without any enclosure structure additionally installed (i.e., open-space environment). Under the condition, the BEV fires continued up until 70 min. Their peak heat release rates (pHRR) were measured to be in the range of 6.51 to 7.25 MW, which were slightly lower than ICEV's (7.66 MW) but higher than FCEV's (5.99 MW). The total heats released (THR) from the BEV fires were measured to be in a range of 8.45 to 9.03 GJ, which were also located in between than smaller ICEVs' (8.08 GJ) and greater FCEV's (10.82 GJ).

In the BEV fires, the major contribution to the quantity of heat release rate was determined by the combustion of the conventional materials of the BEV body (pHRR: 7.81 MW, THR: 7.53 GJ), rather than by that in the LIB pack (pHRR: 1.54 MW, THR: 1.30 GJ). However, as a jet fire intensively discharged from the LIB pack, it accelerated flame spreading to adjacent combustible components, thereby leading to a rapid growth of whole car-fire. The growth parameter for this BEV fire was estimated to be 0.020 (fast medium) which was greater than that for another BEV fire unassociated with jet flames (0.0085, slow medium).

The findings discussed in this study could contribute mainly to the activities of first responders to BEV fire accidents and secondarily to revisiting the safety of existing or new designs of car-parking related structures. For the first responders, BEV fires originating from thermal runaway of LIB packs would be more hazardous than those derived from elsewhere, due to late human awareness of flames and their rapid development once ignited. For the reconsideration of safety, approximately 30 MJ/kg of the average effective heat of combustion can be used to quantify BEV fires. In the context of this, a LIB pack has a high property (approximately 45.9 MJ/kg) which is comparable to that of combustible fuels (e.g., *n*-Pentane with 45.69 MJ/kg).

Funding

The author(s) disclosed receipt of the following financial support for the research, authorship, and/or publication of this article: This project is funded by NFA(National Fire Agency) and KEIT(Korea Evaluation Institute of Industrial Technology) through R&D programme on Development of Fire Safety Technologies for Emergency Response to Fire Hazards (No. 20008021).

Fig. A2. Photos of the specimen status at the critical events in Test 4.

CRediT authorship contribution statement

Sungwook Kang: Methodology, Investigation, Data curation, Visualization, Software, Writing – original draft. **Minjae Kwon:** Data curation, Formal analysis, Project administration. **Joung Yoon Choi:** Funding acquisition, Formal analysis, Resources, Project administration, Supervision. **Sengkwan Choi:** Funding acquisition, Conceptualization, Methodology, Validation, Writing – review & editing.

Declaration of Competing Interest

The authors declare that they have no known competing financial interests or personal relationships that could have appeared to influence the work reported in this paper.

Data availability

Data will be made available on request.

Appendix

See the Figs. A1 and A2.

References

[1] R. Matulka, The history of the electric car. In: Department of Energy, https://www.energy.gov/articles/history-electric-car, Assessed on 23 Mar 2022.
[2] R. Irle, Global EV sales for 2021. In: EV Volumes.com, https://www.ev-volumes.com/country/total-world-plug-in-vehicle-volumes/, Assessed on 23 Mar 2022.
[3] J. Edmondson, A. Holland, R. Collins, L. Gear, Electric car sales, models & technologies database, IDTechEx, https://www.idtechex.com/en/research-report/electric-car-sales-models-and-technologies-database/824, Assessed on 23 Mar 2022.
[4] B. Johnson, Sony flamed for battery bungle, https://www.theguardian.com/technology/2006/aug/31/sony.guardianweeklytechnologysection, Assessed on 11 Nov 2022.
[5] S. Gibbs, Samsung suspends sales of Galaxy Note 7 after smartphones catch fire, https://www.theguardian.com/technology/2016/sep/02/samsung-recall-galaxy-note-7-reports-of-smartphones-catching-fire, Assessed on 11 Nov 2022.
[6] Y.H. Kim, How to resolve electric vehicle fires, National Fire Research Institute of Korea, In: Fire Protection News, https://www.fpn119.co.kr/171590, Assessed on 23 Mar 2022.
[7] Mangs J, Keski-Rahkonen O. Characterization of the fire behaviour of a burning passenger car. Part I: Car fire experiments, Fire Safety Journal 1994;23:17–35.
[8] Shipp M, Spearpoint M. Measurements of the severity of fires involving private motor vehicles. Fire Mater 1995;19:143–51.
[9] D. Joyeux, J. Kruppa, L.-G. Cajot, J.-B. Schleich, P. van de Leur, L. Twilt, Demonstration of real fire tests in car parks and high buildings, European Commission, Technical Steel Research, Final Report, EUR-29466 EN, 2002.
[10] Y. Shintani, N. Kakae, K. Harada, H. Masuda, W. Takahashi, Experimental investigation of burning behavior of automobiles, 6th Asia-Oceania Symposium on Fire Science and Technology, Daegu, Korea, 17-20 March 2004.

[11] Okamoto K, Watanabe N, Hagimoto Y, Chigira T, Masano R, Miura H, et al. Burning behavior of sedan passenger cars. Fire Saf J 2009;44:301–10.
[12] N. Watanabe, O. Sugawa, T. Suwa, Y. Ogawa, M. Hiramatsu, H. Tomonori, H. Miyanoto, K. Okamoto, M. Honma, Comparison of fire behaviors of an electric-battery-powered vehicle and gasoline-powered vehicle in a real-scale fire test, 2nd International Conference on Fires in Vehicles - FIVE 2012, pp.195-205, Chicago, USA, September 27-28, 2012.
[13] Tohir MZM, Spearpoint M. Distribution analysis of the fire severity characteristics of single passenger road vehicles using heat release rate data. Fire Sci Rev 2013;2:5–30.
[14] A. Lecocq, M. Bertana, B. Truchot, G. Marlair, Comparison of the fire consequences of an electric vehicle and an internal combustion engine vehicle, 2nd International Conference on Fires in Vehicles - FIVE 2012, pp.183-194, Chicago, USA, September 27-28, 2014.
[15] Spearpoint M, Tohir MZM, Abu AK, Xie P. Fire load energy densities for risk-based design of car parking buildings. Case Studies in Fire Safety 2015;3:44–50.
[16] C. Lam, D. MacNeil, R. Kroeker, G. Lougheed, G. Lalime, Full-scale fire testing of electric and internal combustion engine vehicles, 4th International Conference on Fire in Vehicles, Baltimore, USA, October 5-6, 2016.
[17] Dahlberg M. The SP industry calorimeter for rate of heat release measurements up to 10 MW. SP Report 1992;1992:43.
[18] R.A. Bryant, M.F. Bundy, The NIST 20 MW calorimetry measurement system for large-fire research, NIST Technical Note 2077, 2019.
[19] Sun P, Huang X, Bisschop R, Niu H. A review of battery fires in electric vehicles. Fire Technol 2020;56:1361–410.
[20] C. Huggett, Estimation of rate of heat release by means of oxygen-consumption measurements, Fire and Materials 4(2):61-65.
[21] ISO 24473:2008, Fire tests – Open calorimetry – Measurement of the rate of production of heat and combustion products for fires of up to 40 MW, International Organization for Standardization, 2008.
[22] Bryant RA, Bundy MF. The NIST 20 MW calorimetry measurement system for large-fire research, NIST Technical Note 2077. National Institute of Standards and Technology 2019. https://doi.org/10.6028/NIST.TN.2077.
[23] Hadjisophocleous GV, Mehaffey JR. Fire Scenarios. Chap. 38, SFPE Handbook of Fire Protection Engineering. fifth ed.,. New York: Springer; 2016.
[24] Wang Y, Burgess I, Wald F, Gille M. "Introduction to enclosure fire dynamics" Chap 3. Performance-Based Fire Engineering of Structures: CRC Press Taylor & Francis Group NW; 2013.
[25] Drysdale D. "Fire Science and Combustion" Chap 1, An Introduction to Fire Dynamics third edi. John Wiley & Sons West Sussex UK; 2021.
[26] Walters RN, Hackett SM, Lyon RE. Heats of combustion of high temperature polymers. Fire Mater 2000;24(5):245–52.
[27] Mei J, Liu H, Chen M. Experimental study on combustion behaviour of mixed carbonate solvents and separator used in lithium-ion batteries. J Therm Anal Calorim 2020;139:1255–64.